Supporting information to

Stable Pt clusters anchored to monovacancies on graphene sheets

Bharat K. Medasani [†], *Jun Liu* [‡], *Maria L. Sushko* [†,*]

† Physical and Computational Sciences Directorate, ‡ Energy and Environment Directorate,

Pacific Northwest National Laboratory, Richland WA 99354, USA

1. METHODS

The DFT calculations were performed with both Plane Wave and Gaussian Plane Wave (GPW) methods using VASP[1] and CP2K[2] codes respectively. We used PBE[3], a semi-local exchange-correlation functional. In CP2K, frozen core approximation with GTH pseudopotentials[4] and Gaussian double zeta with polarization (DZVP) basis sets[5] were utilized. The structures were optimized under periodic boundary conditions using a real space integration grid cutoff of 200 Ry in CP2K and 400 eV energy cutoff in VASP. To minimize interaction between periodic images of Pt nanocluster, a 17.36×17.21 Å^2 rectangular graphene (7×4) supercell and 14.82 Å $\times$ 14.82 Å hexagonal graphene (6×6) supercell was used for 13 atom Pt cluster (Pt13) and Pt dimer, respectively.

The morphologies of Pt13 nanoparticles decorating relaxed defective graphene were globally optimized using a revised Basin Hopping[6] algorithm, implemented in ASE[7] and TSASE[8] packages. The lowest energy gaseous phase Pt13 structure reported in Ref.[9] (Figure 1b) was used as the starting structure for Pt13 nanoparticles. The nanoparticle was randomly rotated and positioned with the closest Pt atom at a distance $\geq$ 2 Å above the graphene sheet. The Basin Hopping was performed for 300 steps at 1000K for each initial cluster structure and orientation. Random displacements with uniform distribution ranging from [-0.5 Å, 0.5 Å] were applied to Pt

atoms at each step and the Pt13 nanoparticles were locally optimized until the root mean square residual force on the atoms was smaller than 0.05 eV/Å^2. To speed up global optimization process, Gaussian basis set with 3 exponents for *s* and *p* orbitals and optimized for fast calculations [10] was used for C atoms. A short range DZVP basis set was used for Pt atoms. Finally, the lowest energy structures from global optimization process were reoptimized using plane wave DFT for further analysis.

The figures in the Supplementary Information are generated using VESTA[11], pymatgen[12] and matplotlib.[13]

2. Defect formation energy

Table S1. Common point defects in graphene and their formation energies

Graphene Defect	Formation Energy (eV)	
	This work	Ref.[14]
Stone Wales (55-77)	4.77	4.5 – 5.3
Monovacancy (5-9)	8.27	7.3 – 7.5
5-8-5 Divacancy	7.92	7.2 – 7.9
555-777 Divacancy	7.24	6.4 – 7.5
5555-6-7777 Divacancy	7.58	7.0

3. Analysis of coordination number in Pt13 clusters decorating defects in graphene

To characterize the morphologies of low energy Pt13 clusters decorating graphene, we calculated a) Pt-Pt radial distribution function, and b) Pt-Pt coordination numbers (FIG. **S1**). In FIG. **S1**, *"ico"* and *"low"* corresponds to the gaseous phase icosahedral and optimal[9] structures and the rest of the keywords identify the Pt13 nanoparticles by the defect on which they are adsorbed. In FIG. **S1**a, the radial distribution function from the centroid of the nanoparticle is plotted as a histogram plot with a bin width of 0.1 Å on 0.3 Å spaced grid. It can be noticed that for *"ico"*, 1 atom is on the centroid and all the remaining atoms are equidistant from the centroid. For the remaining nanoparticle morphologies, the absence of Pt atoms near the centroid imply that there are no central Pt atoms and the nanoparticles no longer exhibit the closed packed structure. It can be inferred from the plot that Pt13 adsorbing on vacancy and 555-777 divacancy

have elongated shapes. The compactness of other nanoparticles is similar to the low symmetry gaseous global minima[9] of Pt13.

Coordination number histograms with and without taking C atoms into account are plotted in (b) and (c) of FIG. **S1** respectively. 2.5 Å and 3.1 Å were used as cutoff distances for C-Pt and Pt-Pt distances, respectively. When C atoms are included as neighbors in generating the coordination number histogram, the distribution of coordination numbers (FIG. **S1**b) is somewhat similar to that of the gaseous phase global minima of Pt13. Whereas gaseous phase Pt13 exhibits narrow distribution of coordination numbers ranging from 3-6, Pt13 binding to graphene defects have a maximal coordination number of 8 and the Pt13 decorating pristine graphene has 7 as maximal coordination number. Without considering C as neighbors, the coordination numbers of graphene supported Pt13 have a peak in the coordination number distribution in between 3-5 followed by a tail up to 8 as coordination number.
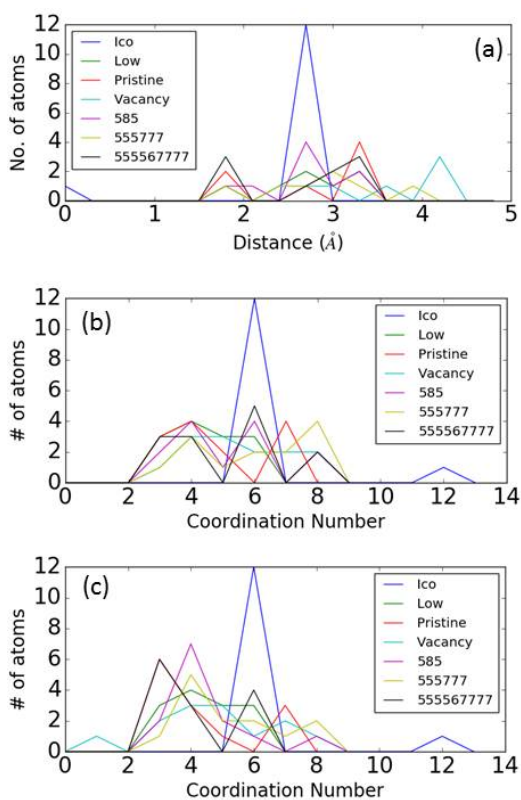

FIG. S1. (a) Radial distribution function from the centroid of nanoparticle, and (b and c) histograms of Pt coordination numbers with and without C atoms for the Pt13 nanoparticles in gaseous and graphene support.

4. Electronic structure of graphene sheets decorated with Pt13 clusters

The charge distribution plots in FIG. **S** show that the Pt atoms in the vicinity of graphene sheet participate in the binding process in confirmation with the conclusions derived in Ref.[15]. The electronic density of states (DOS) plotted in FIG. **S** for C p-orbitals before and after Pt13 decoration show that the defect states below the Fermi level are significantly broadened to a feature-less DOS. The DOS plots corresponding to Pt d-orbitals shown in Fig. S2 show that the Pt13 nanoparticles decorating graphene have DOS features that match with those of the gaseous phase optimal Pt13 configuration. When compared to the DOS plot of icosahedral Pt13 nanoparticles, optimal nanoparticles can be characterized with continuous and irregular d-DOS below the Fermi level. Interestingly, only the DOS of the Pt13 decorating 5-8-5 defect, which has the lowest formation energy, exhibits spin symmetry.
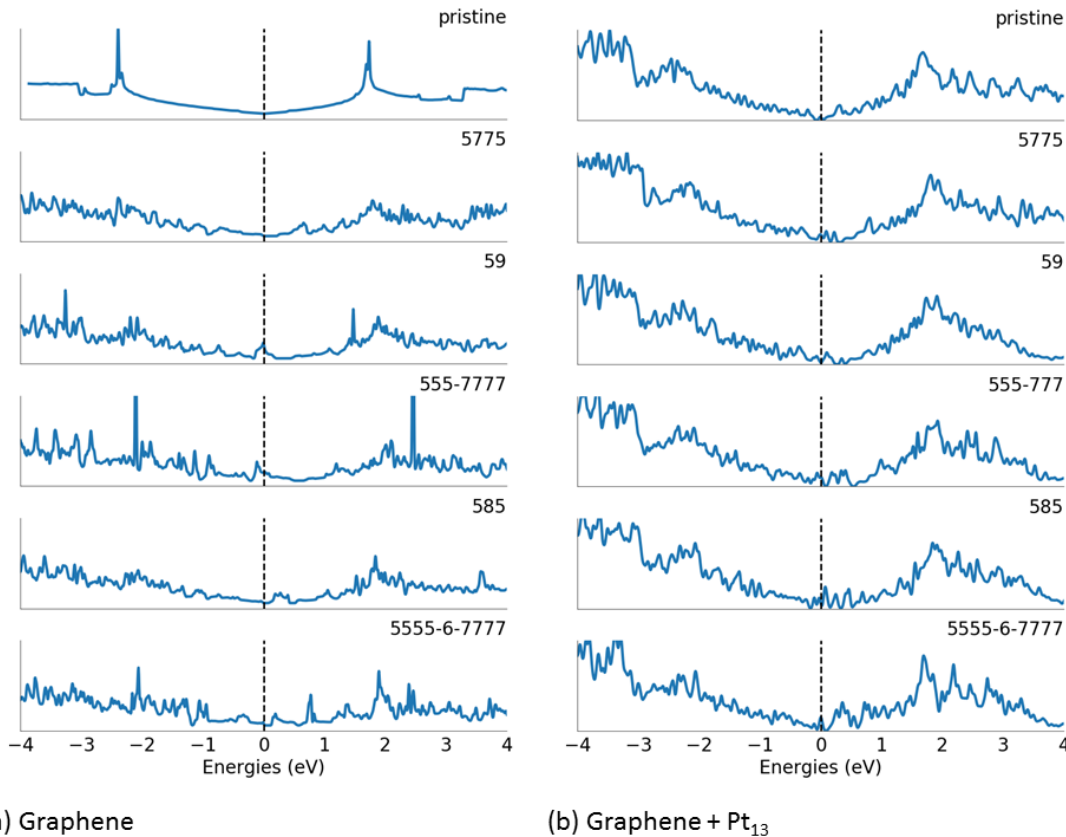

(a) Graphene (b) Graphene + Pt$_{13}$

FIG. S2. Electronic density of states (DOS) plot in (a) pristine and defective graphene, (b) pristine and defective graphene with Pt13 decoration. The DOS plots are smoothened with a Gaussian kernel of 0.02 eV width.
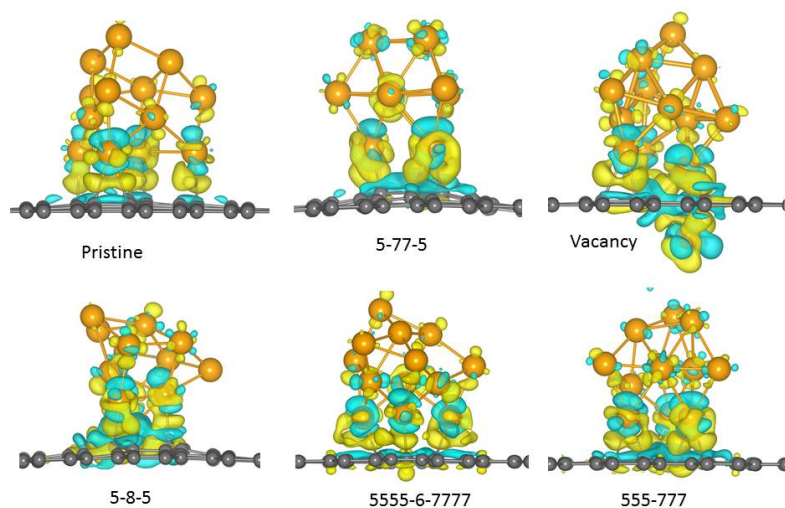
FIG. S3. Charge density difference plots with the isosurfaces corresponding to 0.004 electrons/Bohr^3. Yellow and green colors represent excess and deficit charge regions, respectively.
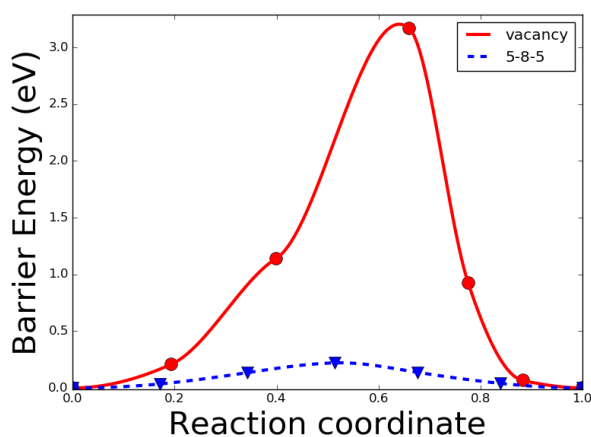
5. Pt diffusion calculations

FIG. S4. Transition state plots of Pt diffusion through monovacancy and 5-8-5 divacancy. Proper convergence of NEB calculation could not be obtained for vacancy.

REFERNCES:

1. G. Kresse, and J. Hafner: Ab initio molecular dynamics for liquid metals. Phys. Rev. B 47, 558 (1993).

2. J. Hutter, M. Iannuzzi, F. Schiffmann, and J. VandeVondele: CP2K: Atomistic Simulations of Condensed Matter Systems. Wiley Interdiscip. Rev. Comput. Mol. Sci. 4, 15 (2014).

3. J. P. Perdew, K. Burke, and M. Ernzerhof: Generalized Gradient Approximation Made Simple. Phys. Rev. Lett. 77, 3865 (1996).

4. S. Goedecker, M. Teter, and J. Hutter: Separable dual-space Gaussian pseudopotentials. Phys. Rev. B 54, 1703 (1996).

5. J. VandeVondele, and J. Hutter: Gaussian basis sets for accurate calculations on molecular systems in gas and condensed phases. J. Chem. Phys. 127, 114105 (2007).

6. D. J. Wales, and J. P. K. Doye: Global Optimization by Basin-Hopping and the Lowest Energy Structures of Lennard-Jones Clusters Containing up to 110 Atoms. J. Phys. Chem. A 101, 5111 (1997).

7. S. R. Bahn, and K. W. Jacobsen: An object-oriented scripting interface to a legacy electronic structure code. Comput. Sci. Eng. 4, 56 (2002).

8. R. Terrel, S. Chill, P. Xiao, J. Duncan, S. Stauffer, R. Bandy, and G. Henkelman: TSASE: Transition State Library for ASE. Retreived Sept 18, 2017, http://theory.cm.utexas.edu/tsase/

9. M. J. Piotrowski, P. Piquini, and J. L. F. Da Silva: Density functional theory investigation of 3d, 4d, and 5d 13-atom metal clusters. Phys. Rev. B 81, 155446 (2010).

10. S. Z. Eeuwe, H. Nils, K. Alan, E. G. Martin, and B. Ulf von: Optimized Gaussian basis sets for Goedecker–Teter–Hutter pseudopotentials. Model. Simul. Mater. Sci. Eng. 17, 015009 (2009).

11. K. Momma, and F. Izumi: VESTA 3 for three-dimensional visualization of crystal, volumetric and morphology data. J. Appl. Crystallogr. 44, 1272 (2011).

12. S. P. Ong, W. D. Richards, A. Jain, G. Hautier, M. Kocher, S. Cholia, D. Gunter, V. L. Chevrier, K. A. Persson, and G. Ceder, Python Materials Genomics (pymatgen): A robust, open-source python library for materials analysis. Comput. Mater. Sci. 68, 314 (2013).

13. J. D. Hunter: Matplotlib: A 2D graphics environment. Comput. Sci. Eng. 9, 90 (2007).

14. F. Banhart, J. Kotakoski, and A. V. Krasheninnikov: Structural Defects in Graphene. ACS Nano 5, 26 (2011).

15. I. Fampiou, and A. Ramasubramaniam: Binding of Pt Nanoclusters to Point Defects in Graphene: Adsorption, Morphology, and Electronic Structure. J. Phys. Chem. C 116, 6543 (2012).